AFRL-SR-AR-TR-04-

0413

REPORT DOCUMENTATION PAGE

1. REPORT DATE (DD-MM-YYYY)	2. REPORT TYPE	3. DATES COVERED (From - To)
12-07-2004	Final report	2-1-02 to 12-31-03

4. TITLE AND SUBTITLE

"Completion of a High-T_c Hand-held SQUID System and Development of Small High-Fill-Factor Coils for Application to Non-Destructive Evaluation"

5a. CONTRACT NUMBER

5b. GRANT NUMBER
F49620-02-1-0115

5c. PROGRAM ELEMENT NUMBER

6. AUTHOR(S)
Frederick C. Wellstood

5d. PROJECT NUMBER

5e. TASK NUMBER

5f. WORK UNIT NUMBER

7. PERFORMING ORGANIZATION NAME(S) AND ADDRESS(ES)

Frederick C. Wellstood
Department of Physics
University of Maryland
College Park, Maryland,
20742-4111

8. PERFORMING ORGANIZATION REPORT NUMBER

9. SPONSORING / MONITORING AGENCY NAME(S) AND ADDRESS(ES)
AFOSR/PKC (ATTN: Wendy Weon)
4015 Wilson Blvd.
Room 713
Arlington, VA 22203-1954 pkcontracting@afosr.af.mil

20040810 024

12. DISTRIBUTION / AVAILABILITY STATEMENT

Distribution Statement A: unlimited

13. SUPPLEMENTARY NOTES

14. ABSTRACT

This project had two main objectives. The first objective was to complete the construction and testing of a high-fill factor, small-coil SQUID system that will allow us to feed a straight wire or flowing medium through a small coil that is tightly coupled to a SQUID. A prototype high-Tc SQUID based cryo-cooled system was designed, built and operated. The goal for this "flow-through" system was to determine whether it will be useful for finding defects in Cu-clad NbTi wire or for other applications involving flowing media. Test copper wire samples up to 2 meters in length were pulled through apparatus at speeds up to a m/s and double frequency subtraction technique was exploited to remove motional artifacts. The second objective was to complete the construction of a hand-held high-Tc SQUID system that was developed by SQM, Inc, determine the feasibility of this approach to building a hand-held SQUID system, and test its applicability to NDE of metal parts. Tests on the cryo-cooler revealed a poor connection to the cryo battery and vibrations from the sterling cycle cryo-cooler were judged to be too large for the system to run while the refrigerator was operating.

15. SUBJECT TERMS

16. SECURITY CLASSIFICATION OF:			17. LIMITATION OF ABSTRACT	18. NUMBER OF PAGES	19a. NAME OF RESPONSIBLE PERSON
a. REPORT	b. ABSTRACT	c. THIS PAGE			19b. TELEPHONE NUMBER (include area code)

8-4-04

Final Report

on

"Completion of a High-T_c Hand-held SQUID System and Development of Small High-Fill-Factor Coils for Application to Non-Destructive Evaluation"

AFOSR Project number F49620-02-1-0115

July 14, 2004

PI: Fred Wellstood

Associate Professor

Department of Physics

University of Maryland

College Park, MD 20742-4111

301-405-7649

well@squid.umd.edu

Outline

1. Project Summary
2. Flow-Through System
3. Hand-Held System
4. Personnel
5. Chapter 9 from the Thesis of Su Young Lee on NDE using SQUID microscopes

1. Project Summary

The AFOSR funded project entitled "Completion of a High-T_c Hand-held SQUID System and Development of Small High-Fill-Factor Coils for Application to Non-Destructive Evaluation" had two main objectives. The first objective was to complete the construction and testing of a high-fill factor, small-coil SQUID system that will allow us to feed a straight wire or flowing medium through a small coil that is tightly coupled to a SQUID. A prototype high-Tc SQUID based cryo-cooled system was designed, built and operated. The goal for this "flow-through" system was to determine whether it will be useful for finding defects in Cu-clad NbTi wire or for other applications involving flowing media. Test copper wire samples up to almost 6 meters in length were pulled through apparatus at speeds up to 1.4 m/s and double frequency subtraction technique was exploited to remove motional artifacts.

The second objective was to complete the construction of a hand-held high-Tc SQUID system that was developed by SQM, Inc, determine the feasibility of this approach to building a hand-held SQUID system, and test its applicability to NDE of metal parts. Tests on the cryo-cooler revealed a poor connection to the cryo battery and vibrations from the sterling cycle cryo-cooler were judged to be too large for the system to run while the refrigerator was operating.

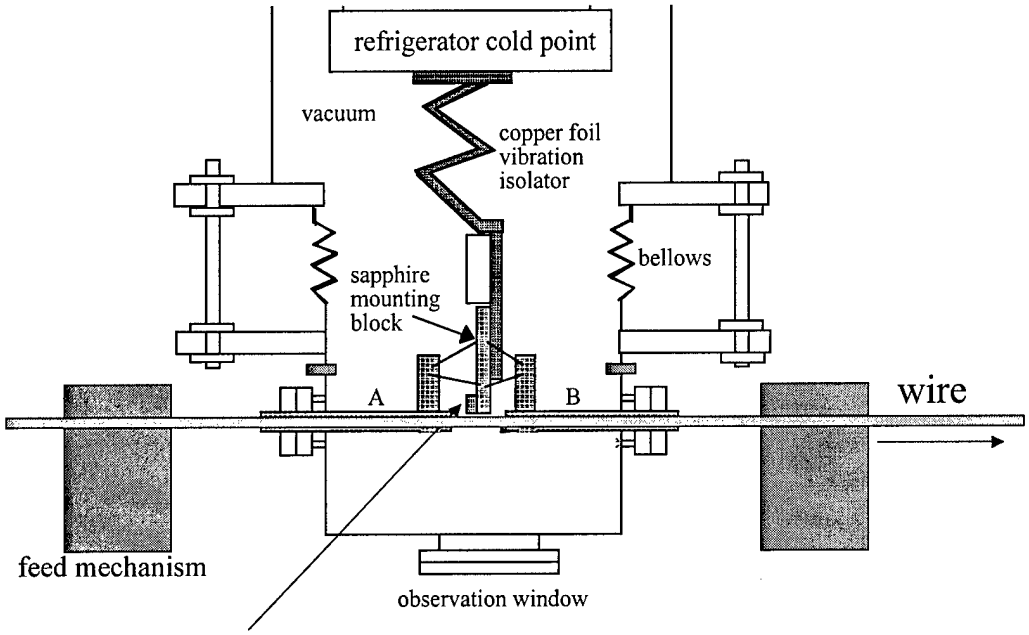

Fig. 1. Schematic of the layout for the flow-through system.

2. Flow-Through system

Figure 1 shows a schematic for our first design for the flow-through SQUID system, illustrating the basic idea behind this instrument. A small high-Tc SQUID is attached to a cold finger which is suspended in vacuum and brought in close proximity to a thin-walled tube that pierces through the vacuum chamber. Solid wires or flowing material can be fed through the tube and changes in magnetic response are detected using the SQUID. In the current design, the tube diameter is about 3 mm, sufficiently large to pass a Cu-clad NbTi MRI wire. A set of bellows will be used to control the spacing between the outer wall of the tube and the SQUID - it is essential that they be close to each other, to get good S/N and resolution, but not touch, in order to prevent heating of the SQUID or cooling of the tube.

We note that in this design, the tube does not pass through the SQUID chip, but right next to it. Ultimately, we will build a system where the tube is brought right through a hole in the chip to ensure good coupling to the SQUID. However, this is considerably more difficult to build, and so as a first step, we have chosen a somewhat simpler system which will let us test the main idea behind the system as well as its components, including the SQUID, the tube, the adjusting mechanism and the cryogenics.

The most critical part of the flow-through system is the thin-walled tube. It needs to be

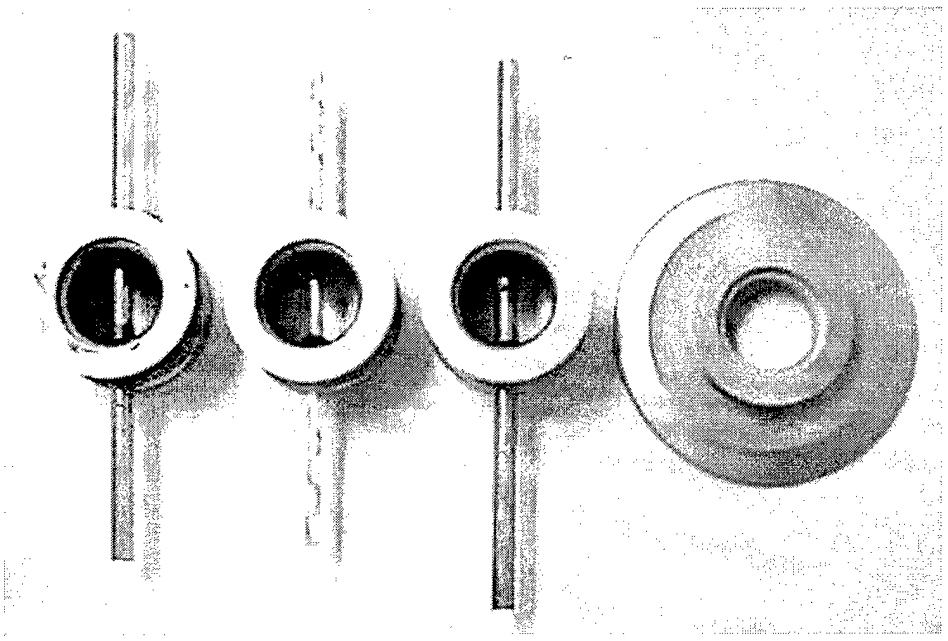

Fig. 2. Thin-walled tubes epoxied into vacuum test fixtures and a mating flange to the cryo-cooled SQUID system. The middle tube is the paralene-C coated Mylar tube used in the prototype.

thin in order to allow the SQUID to be brought close to the flowing sample, but it needs to be strong enough that it can withstand vacuum and contact with a moving MRI wire. In early 2002 we obtained several samples of tubes which we have tested for suitability. All of the tubes have been obtained, at no cost, from Stone Industries in College Park, Maryland. In late 2002, we also obtained four Mylar tubes that we had coated with 25-50 μm of Paralene C by Paratronix, Inc, in Attleboro, MA. This coating is used to improve vacuum performance in thin-walled particle radiation detectors. Figure 2 shows 3 tubes that have been epoxied into a vacuum test fixture. We vacuum test each tube by connecting the assemblies to a Helium leak-detector. We expected to see lower vacuum leak rates, and in fact these tubes have about a n order of magnitude lower leak rate than the uncoated tubes (see Table 1 below). At this point, the Mylar tube #13 in Table 1 is the best and appears to be adequate for our purposes. In particular, it has a very low leak rate. In addition, it is fairly tough and does not appear to be damaged by sliding cu-clad wire samples back and forth inside it.

After settling on a suitable thin-walled tube, we constructed a new YBCO bi-crystal SQUID tip and assembled our first prototype flow-through system by using our existing cryo-cooled SQUID microscope as the platform. We attached the tube test assembly to the bottom of the cryo-cooled SQUID microscope, in place of the thin-window nose cone assembly. Figure 3 shows a view of the completed assembly. The bottom of the flange is capped off with a thick view port window (see Fig. 3).

The existing window positioning mechanism in the microscope can then be used for controlling the separation between the SQUID and the tube. This design and construction was simple, once we obtained a working SQUID tip. In the present set-up, the SQUID is a z-type.

To align the SQUID with we use a microscope to look through the bottom view port at a

Table 1. Dimensions and helium leak rates of thin-walled tubes

		Wall thickness (μm)	O.D. (mm)	He leak rate (10^{-6} std cc/s)
1	mylar	50-75	3.35	4
2	kapton	75-100	3.84	3
3	kapton	75-100	2.85	3
4	Kapton - wrapped in cellophane	75-100	4.19	Gross leak
5	Kapton- Teflon bonded	150	5.94	3
6	Kapton - "Solvent"	75	5.59	6
7	kapton	75-100	4.32	3
8	mylar	90-130	3.51	1.5
9	mylar	100-140	3.61	1
10	mylar	125-150	3.40	1
11	Mylar coated with 25μm of Paralene C	50-75	5.64	0.41
12	Mylar coated with 50μm of Paralene C	50-75	5.64	0.2
13	Mylar coated with 25μm of Paralene C	75-100	3.45	0.13
14	Mylar coated with 50μm of Paralene C	75-100	3.45	0.13

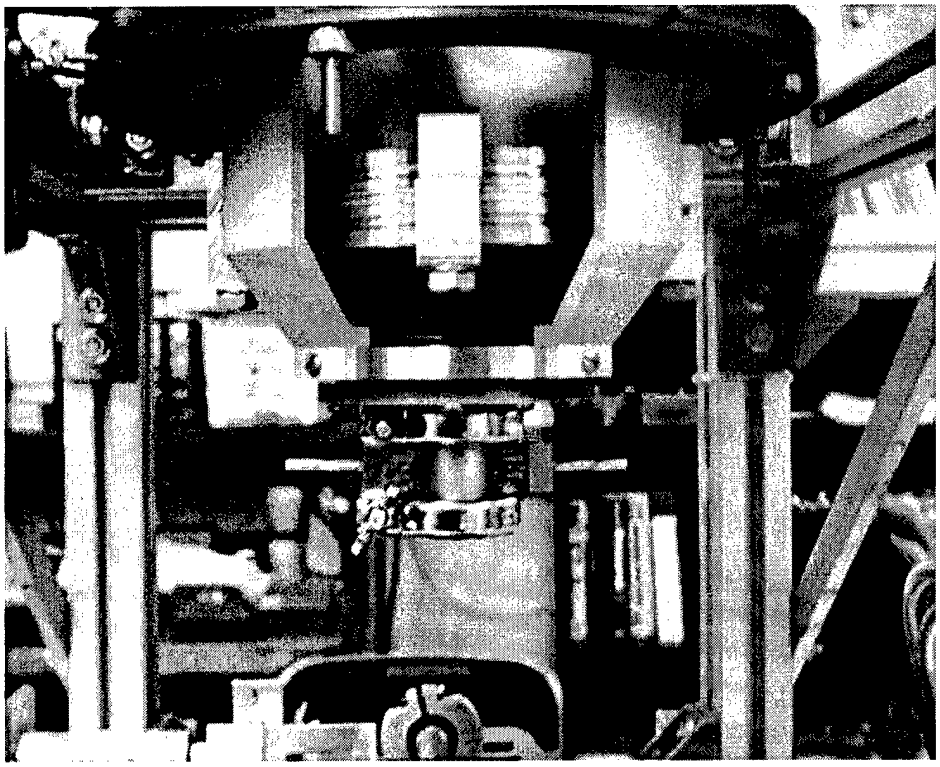

Fig. 3. Completed flow-through prototype showing view of the tube mounted on the Cryo-cooled SQUID system.

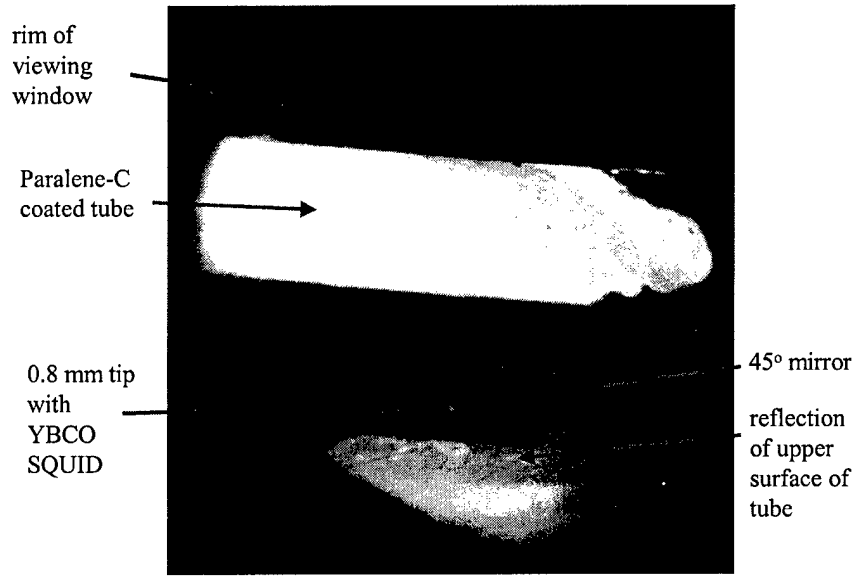

Fig. 4. View of the SQUID tip and tube mounted in the system.

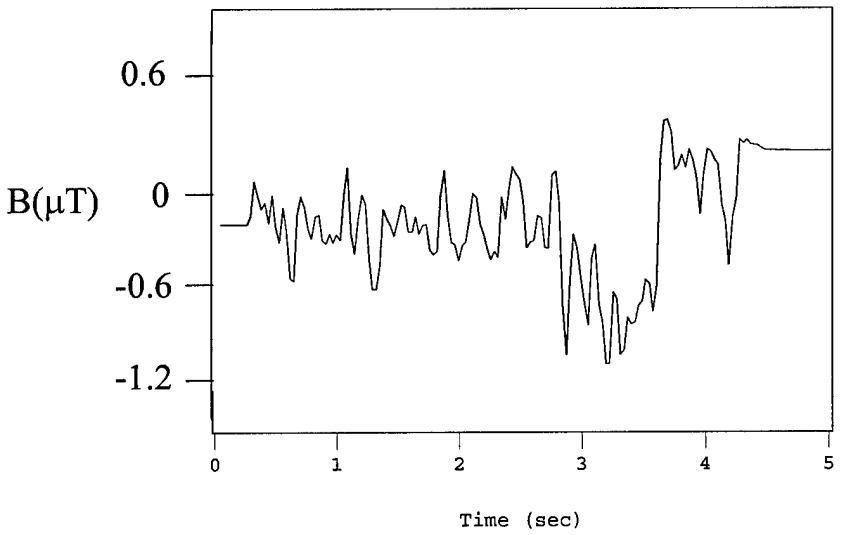

Fig. 5. Fast pull test. A 5.75 m section of thin copper wire with 5 mA of current at 1.245 kHz is pulled through the flow-through system at 1.36 m/s while the SQUID records the field amplitude.

45° mirror mounted inside the flange. The top of the tube and end of the SQUID tip are visible as reflections in the mirror. Figure 4 shows a view of the tube and tip in the mirror, with everything cold and the SQUID locked. We can use the z-adjustment on the window manipulator assembly to bring the tip close to the top of the tube.

We ran a number of tests on the completed prototype. Figure 5 shows the results of pulling a 5.75 m stretch of thin copper wire at 1.36 m/s. In this case the wire was carrying 5 mA of 1.245 kHz current and the SQUID output was fed to a lock-in detector with 100 Hz bandwidth. The significance of this test is that we system was able to maintain lock, despite the rather large motional noise as the wire was pulled through at a good speed. In fact, if we can detect defects at something like 1 m/s, this should be very reasonable for doing km long sections.

As another example of preliminary results, Fig. 6a shows that we were able to obtain a simultaneous high-frequency low-frequency current measurement, and that the difference of these two signals cancelled out the motional artifacts.

The key next step that needs to be verified is that we can detect defects, as we were able to with the SQUID microscope. Given the high-scanning speeds, this may prove to be non-trivial. Figures 6b and 6c, however illustrates why we believe this is not a major barrier. This

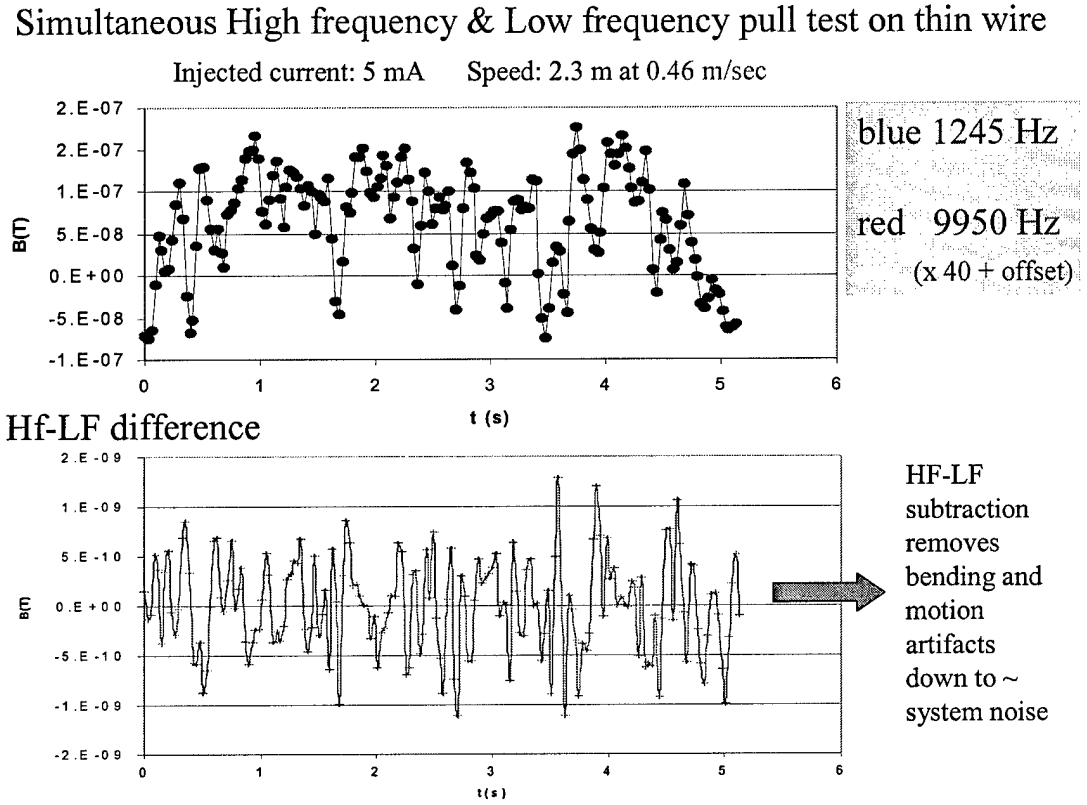

Fig. 6a. Results of simultaneous high-frequency low-frequency pull test on a thin Cu wire showing that the difference cancels out signals from movement of the wire.

image was taken using a multi-channel high Tc SQUID microscope, developed under an earlier funded AFOSR project, and shows results on a test Cu sample that had holes of different sizes drilled into it. The smallest hole in the sample was just 17 mm in radius and was only drilled half-way through the rod. Never the less, the magnetic signal it created is clearly visible, and orders of magnitude above the level of the noise. This same system was used to verify the high-low frequency subtraction technique and used SQUIDs of the same size as in the flow-through system and at about the same distance.

A future stage in this project is to develop a system where the tube passes through a hole in the SQUID chip which is centered on a loop that is coupled to the SQUID. More development work is needed on techniques for drilling the holes. We already have some

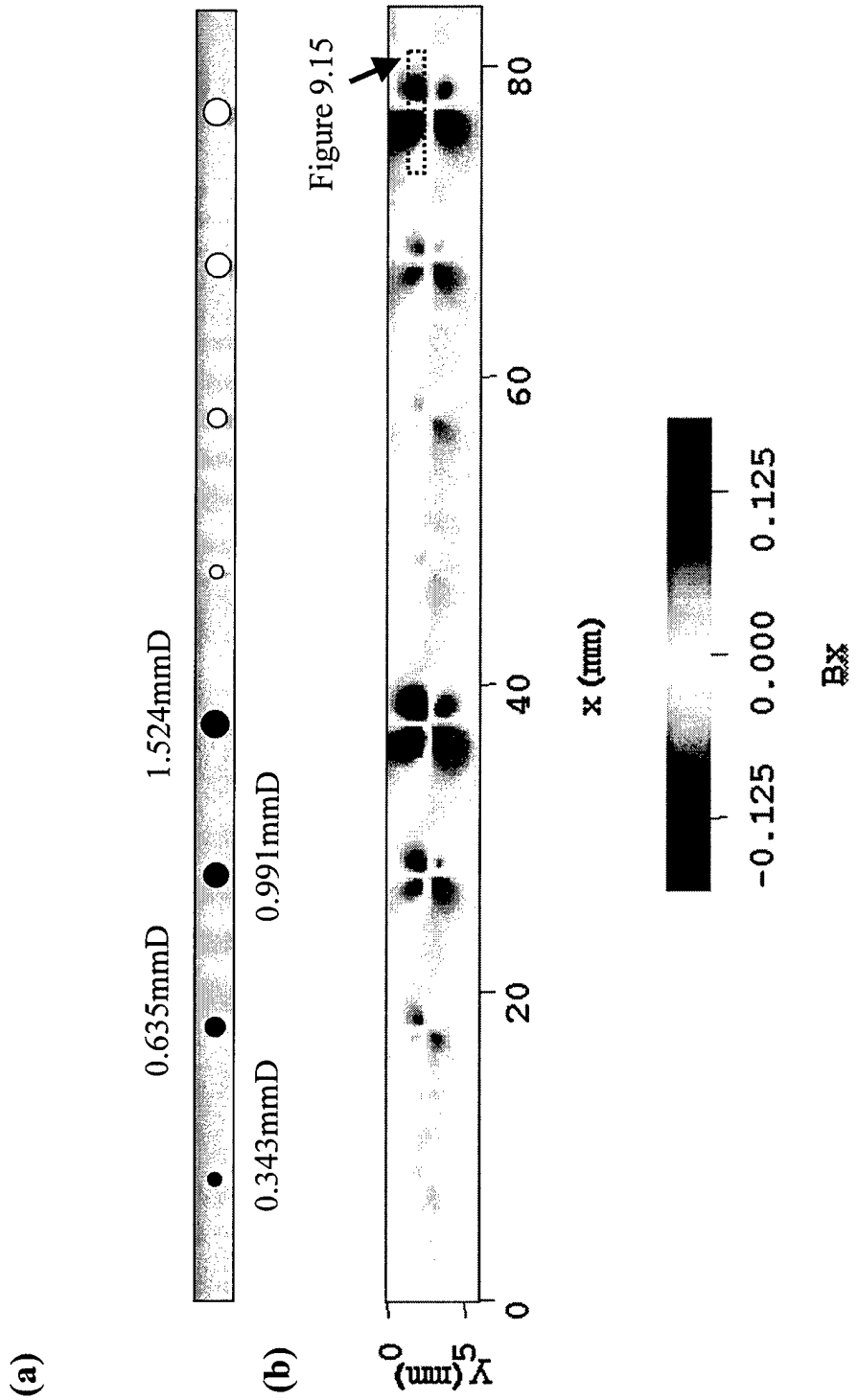

Figure 6 (b) Sketch of brass test sample D with 4 half-through holes and 4 through hole having various hole sizes. (c) Raw magnetic field image of current injected sample D.

experience with this type of process since we need to create such holes for the support structures we use for the thin windows in our SQUID microscopes. However, our experience is with sapphire and not with the $SrTiO_3$ we would use for a bi-crystal SQUID chip, and STO appears to be more brittle. Fortunately, the holes we need are not very fine (of the order of 2-3 mm), so that we should not have too difficult of a time producing them.

3. Hand-held system

The second part of this project involved completing a hand-held SQUID system that was being developed by SQM. The main accomplishments in this part of the project are:

1. We received from SQM the parts of the hand-held system that they did complete. This includes one nearly complete unit (see Fig. 7), the vacuum jacket of a second unit, and a few cryogenic battery masses. A few important pieces were missing, including the controller for the stirling refrigerator, the connectors and wiring harness for the unit, associated vacuum tubes and fitting, and of course the SQUID sensors.

2. We have also received from SQM the lab notebooks and CDs for the project. These have been very helpful, and include items such as the CAD layout for the hand-held unit (see Fig. 8). We have cataloged the items and need to return non-hand-held items to Mrs. Podney.

3. We have done several vacuum tests on the hand-held unit. After replacing a missing seal, we have found the vacuum tightness is acceptable.

4. We disassembled the unit (see Fig. 9) and traced the wiring from the outer wiring feed-though to the top cold-plate of the unit. A set of wiring for a SQUID and thermometer are intact.

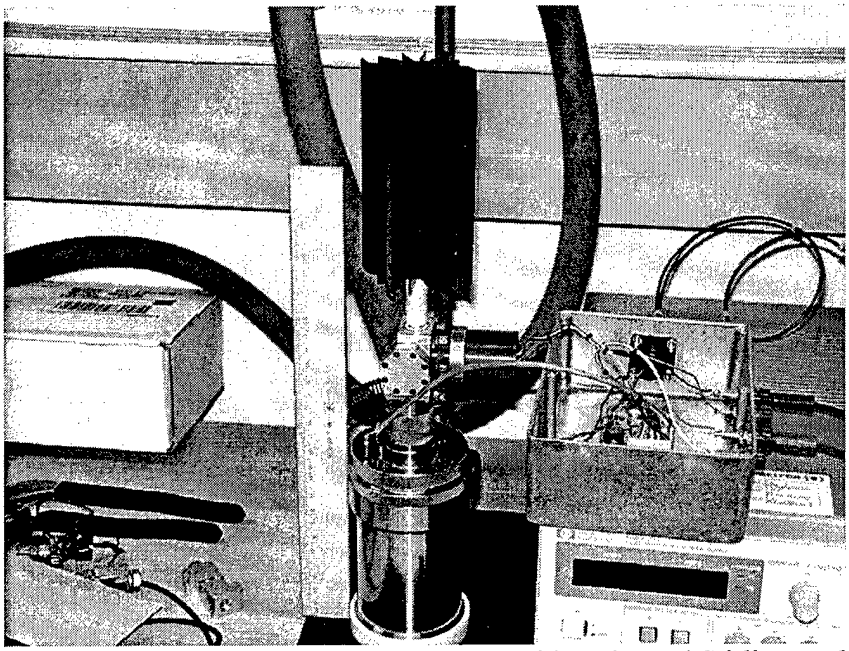

Fig. 7. Photograph of SQM Hand-held SQUID system with recharged Stirling cycle cry-cooler and controller attached.

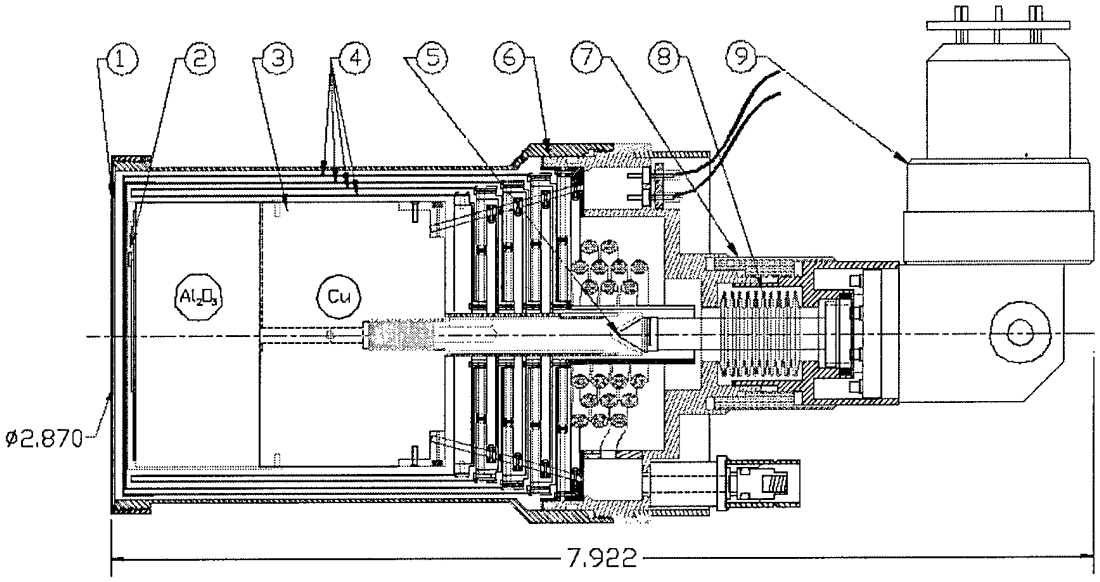

1. sapphire window	4. thermal shields	7. coupling turnbuckle
2. SQUID array	5. refrigerator cold pad	8. bellows
3. cryobattery	6. vacuum jacket	9. microcooler

Fig. 8. CAD diagram of SQM hand-held SQUID system.

5. We found the manufacturer of the Stirling refrigerator, FLIR, who purchased the original company that manufactured the unit. FLIR still supports the product, and we sent the unit off to their engineers to check its gas pressure, test the operation of the unit, and figure out what we need in terms of power cables and a control unit. This process took several months, the resulting delay slowed us down considerably. We did eventually receive a recharged unit and parts for a controller as well as some rudimentary instructions.

6. With the integrity of the vacuum and wiring established, we began to test how the unit cools. After several contacts with the manufacturer, we were able to successfully operate the cryo-refrigerator unit alone. It achieved a base temperature of about 65 K with no thermal load in just a few minutes.

7. We next mounted the refrigerator in the SQM system and attempted to cool the entire unit. This was where we ran into our first significant problem. The unit cooled very slowly and did not get very cold, only reaching 240 K after 5 hours. We then substituted an equivalent 0.7 kg cu mass and ran the system for a couple days, it reached about 115 K in 30 hours. Switching to a 0.36 kg or a 0.09 kg copper mass, we reached about 100 K in 20 hours. We noted that the initial cooling rates, as well as the time to reach base temperature were not scaling with the thermal mass, and concluded that the thermal coupling between the refrigerator and the mass was neither consistent nor good. Inspection of the refrigerator cold-point revealed a brass tip that was held to the stainless steel cold point of the refrigerator by means of a slip ring that was seated in a groove that cut almost all the way through the end of the stainless steel cold point. The numerous boundaries and the loose fit were judged to be the source of the problem with thermal contact.

8. To alleviate the poor contact, we sliced off the end of the stainless steel cold point at the slip ring groove and epoxied the test mass directly to the exposed end of the cold-point. Preliminary tests indicated that the resulting unit cools to at least 85 K, which

would be about adequate for our purposes.

9. We fabricated a YBCO SQUID magnetometer for the system and our planned to operate it on the cold finger with the refrigerator running. Although this will be a magnetometer chip, its small size will allow us to operate it in the unit with minimal shielding. The idea was to compare the SQUID's performance on the hand-held unit directly with the performance of similar sized SQUIDs in our microscopes.

10. However, before we got to this point, we ran into serious problems with the thermal contact again. It turned out that vibrations from the cryo-cooler were, over time, putting stress on the joint between the cold finger and the thermal mass, which caused cracking and progressive failure of the thermal link. Typically after a few hours operation or afew cooldown cycles, the mass would no longer cool. The vibrations from the cryo-cooler, were also a significant worry that would likely prevent operation of a SQUID while the cryocooler was on. Given these now obvious problems, and the long cool-down times when a reasonable sized cryo-battery were used even with a good link, we decided reluctantly to abandon this part of the project.

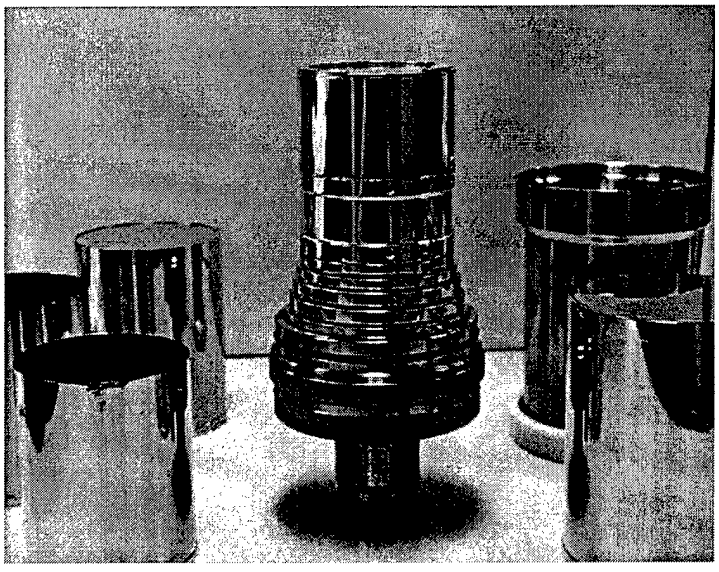

Fig. 9. Photograph of SQM Hand-held SQUID system after outer heat shields and vacuum can have been removed.

In retrospect, the weak point turned out to be the cryo-cooler. For a hand-held system, one needs a small (light weight), magnetically quiet, low vibration system with good cooling power. The chosen unit did not have all of these properties, and it is not clear that a superior replacement is available.

4. Personnel

The main personnel who worked on this project are Dr. John Matthews (post-doc), Cavan Wilk (an undergraduate student), Satheesh Angaiah (graduate student), Vijay Viswanathan (graduate student), and Gus Vlahacos (graduate student). In addition, John Huckans (graduate student) worked on the project during the first summer, Su Young Lee contributed valuable experience and comparison results on the multi-channel SQUID microscope, and Dr. Roberto Ramos assisted with the set up and operation of the cryogenically cooled SQUID system. Su Lee and Maria Aronova (grad students) also helped greatly with set-up and operation of the SQUIDs for the flow-through system as well as getting the SQUID chip on the tip, while Vijay has been responsible for the design and taking data. Sateesh and Gus have been mainly working on the hand-held system.

5. CHAPTER 9 from the Thesis of Su Young Lee on "Fault Detection of Superconducting Wire Using a Scanning SQUID microscope"

This last section of this final report is Chapter 9 from the Thesis of Su Young Lee. It is titled "Fault Detection of Superconducting Wire Using a Scanning SQUID microscope" and concerns results she generated on imaging of defects in NbTi wires and copper test samples using a multi-channel scanning SQUID microscope. The aim of this work was largely to provide

comparison with results on the flow-through system. It also was useful for trying out new ideas and verifying whether a given sample defect would be visible.

9.1 Superconducting wire

Nb-Ti superconducting wire is used to make the coil winding for superconducting magnets of Magnetic Resonance Imaging (MRI) system. The magnet made of the superconducting wire is far more efficient than conventional copper wire and withstand higher magnetic fields. Typical construction of the superconducting wires is to embed a large number of fine filaments in a copper matrix as shown in Fig 9.1. The solid copper gives mechanical stability and provides a path for the large currents in case the superconducting state is lost.

If the defect such as broken Nb-Ti filaments is deep in a core of wire, it can pass inspection on the factory. The superconducting magnet with defect deep inside can be tested only when it is installed and cooled down. If the magnet is determined as fault, then the MRI system is scrapped. That is why accurate detection of the defect without destroying sample is important.

There are 4 main types of defects in the process of manufacturing [1];

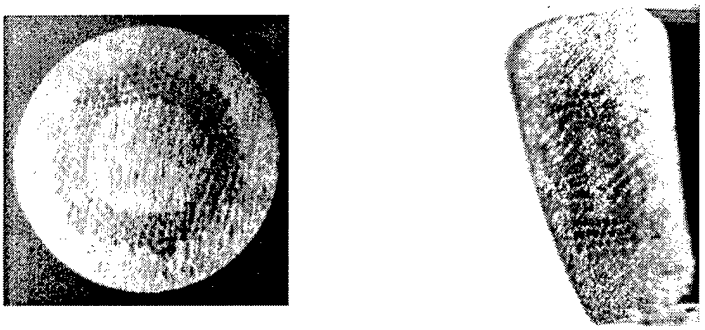

Figure 9.1 Photograph of Nb-Ti superconducting wire with (a) round and (b) rectangular cross section from IGC Inc [2].

(a) Yields: the wire has stretched beyond its elastic limit. The stretch can break the filament in the core or cause crack which Cu cladding fills

(b) Occlusions: Non-conducing grain gets incorporated into core or cladding.

(c) Seams: the wire has been folded over leaving an internal poorly-conducting plane running

(d) Bare spots: the insulating jacket around the wire is missing or has bee rubbed off.

My samples are commercial Nb-Ti from IGC advanced superconductors Inc. [2]. The ratio of copper to superconductor is up to about 7 to 1. It varies depending on application. The superconducting wires have 1~3 mm diameter with round or rectangular cross-section. To prevent electrical shorts, the outside copper is coated with the insulating material. This is the list of my samples which I measured;

i. Sample A has round cross section (1.45 mm Diameter) with the "yield" defect.

ii. Sample B has rectangular cross section (2.29×1.55 mm^2) with the "seam" defect.

iii. Sample C has round cross section (1.45 mm Diameter) with the " yield" defect.

iv. Sample D is homemade Brass test sample 4 through holes and 4 half-through holes with different sizes.

9.2 Old fault detection methods with SQUID

9.2.1 eddy current method

Eddy current method is most common for fault detection of superconducting wires. Figure 9.2 shows the schematic of eddy current method. The 200 turn-coil induce drive field. The drive field induces the eddy current. Another magnetic field is caused by the eddy current. The magnitude and direction of the field is different depending on

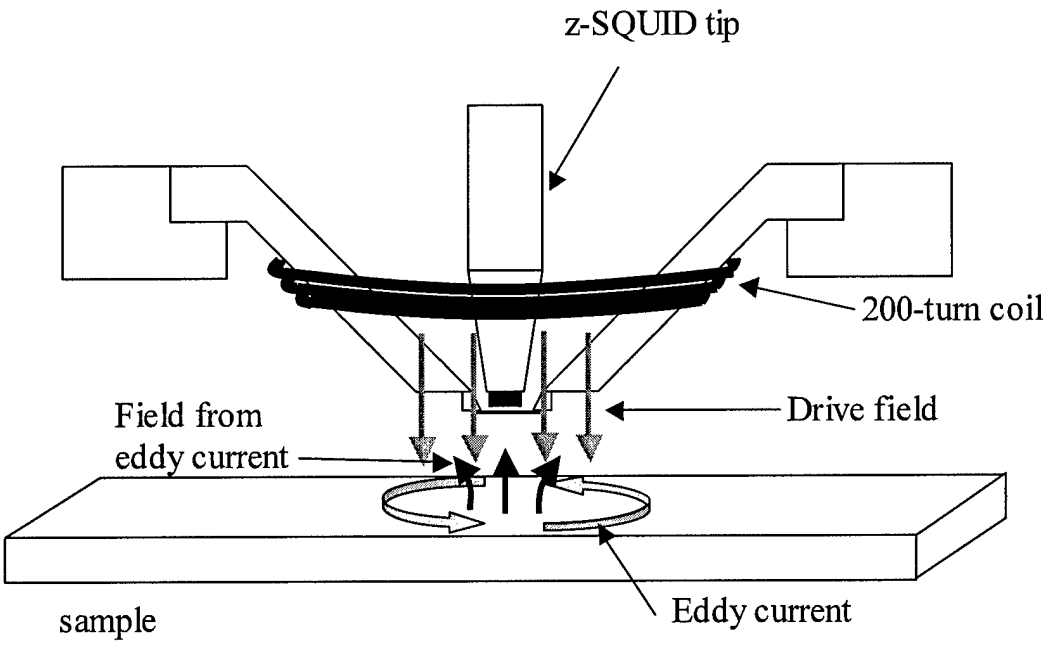

Figure 9.2 Schematics of experimental set-up for eddy current imaging (modified from [3])

the sample geometry. If there is a void inside of the wire, the current flow turning the void, resulting in different direction and magnitude of magnetic field. Since SQUID is very sensitive flux meter, it can detect very slight change. I note that the sample geometry is limited where the penetration depth reaches. The penetration depth is function of frequency. The penetration depth for low frequency current is long, while the penetration depth for high frequency current is short. The relation between the penetration depth and frequency is given by [4],

$$d = \sqrt{\frac{1}{\pi f \mu_0 \sigma}} \qquad (9.1)$$

where μ_0 is the permeability of free space, σ is the conductivity of the wire, and f is the frequency of the applied current.

The magnetic field with the defect is detected by z-SQUID (SQUID loop is parallel to sample plane). Previous member E. Fleet measured the test samples made of artificial defect and real superconducting wire using eddy current method [5]. He could localize the defect in the test samples, but the real defect in superconducting wire didn't appear in eddy current method. To obtain a reasonable signal, large coil and relatively high amplitude and high frequency of the applied current is required. The large coil gives poor spatial resolution. He could not apply high enough amplitude and frequency of current because it caused the SQUID unlock. Low frequency current in the coil cause very weak magnetic field, therefore high enough frequency (maximum frequency not to cause SQUID unlock) is required. The penetration depth of high frequency gives only the shallow surface information of the sample to SQUID. In addition, the induced field is small compared with the drive field and the signal from the wire itself (not defect) is much stronger than the signal from the defect. For these reasons, the defect of superconducting wire did not appear.

9.2.2 Current injection method with z-SQUID

Current injection method is that the current is injected into the sample and SQUID measured the magnetic field from the sample. E. Fleet measured the defect of test samples and the superconducting wire using the method with z-SQUID [4]. One of test sample had cylindrically asymmetric defect and the other had cylindrically symmetric defect. Since the raw magnetic field B_z from wire itself is very strong, taking derivative with respect of y (dB_z/dy) pull out defect features [5,6]. The asymmetric defect of the test sample and the superconducting wire appeared in the derivative of magnetic field image. However, the symmetric defect of the test sample didn't show up because the induced magnetic fields with and without symmetric defect are

identical by the symmetry. Figure 9.3 show the magnetic field and field gradient image of the superconducting wire. The darkest red and blue indicate maximum and minimum value, respectively. As marked with dashed line in Fig. 9.3(b), the defect appeared as a dipole structure, but there are strong signal in the top and bottom because of bending in the wire. The current injection method with the z-SQUID is very sensitive to detecting the defect of the wire, but at the same time it is sensitive to the bending of the wire. Since the actual superconducting wires are not ideally flat, we need to work more to pull out the defect from it.

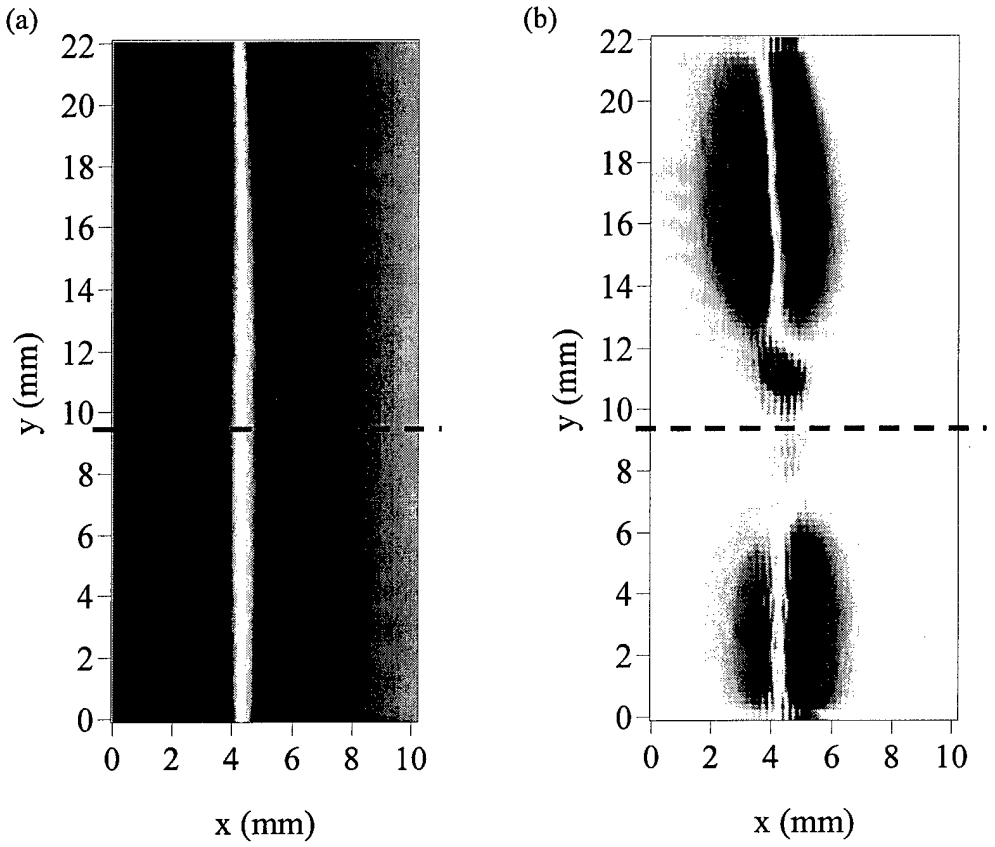

Figure 9.3 (a) Raw magnetic field (B_z) image of current injected superconducting wire using z-SQUID. Reds/Blues indicate +/- 840nT. (b) dB_z/dx calculated from (a). Reds/Blues indicate +25/- 50nT/mm. It is taken by E. Fleet [5].

9.3 current injection method with *x*-SQUID

Main problem of detecting the fault of the wire using the current injection method by z-SQUID was too strong signal from wire itself. While z-SQUID is sensitive to z component of magnetic field, *x*-SQUID is sensitive to *x*-component of magnetic field. Differently from z-SQUID, the direction of wire is very important for *x*-SQUID. If the wire is aligned exactly to

parallel to SQUID loop, then no signal is detected by the x-SQUID. If there is a defect in the wire, then it causes the flow of the current in irregular direction, resulting in x component of the magnetic field, which can be detected by x-SQUID. Since the signal from the current injected wire is weak compared with the signal from the defect, the raw magnetic field data of x-SQUID can localize the defect.

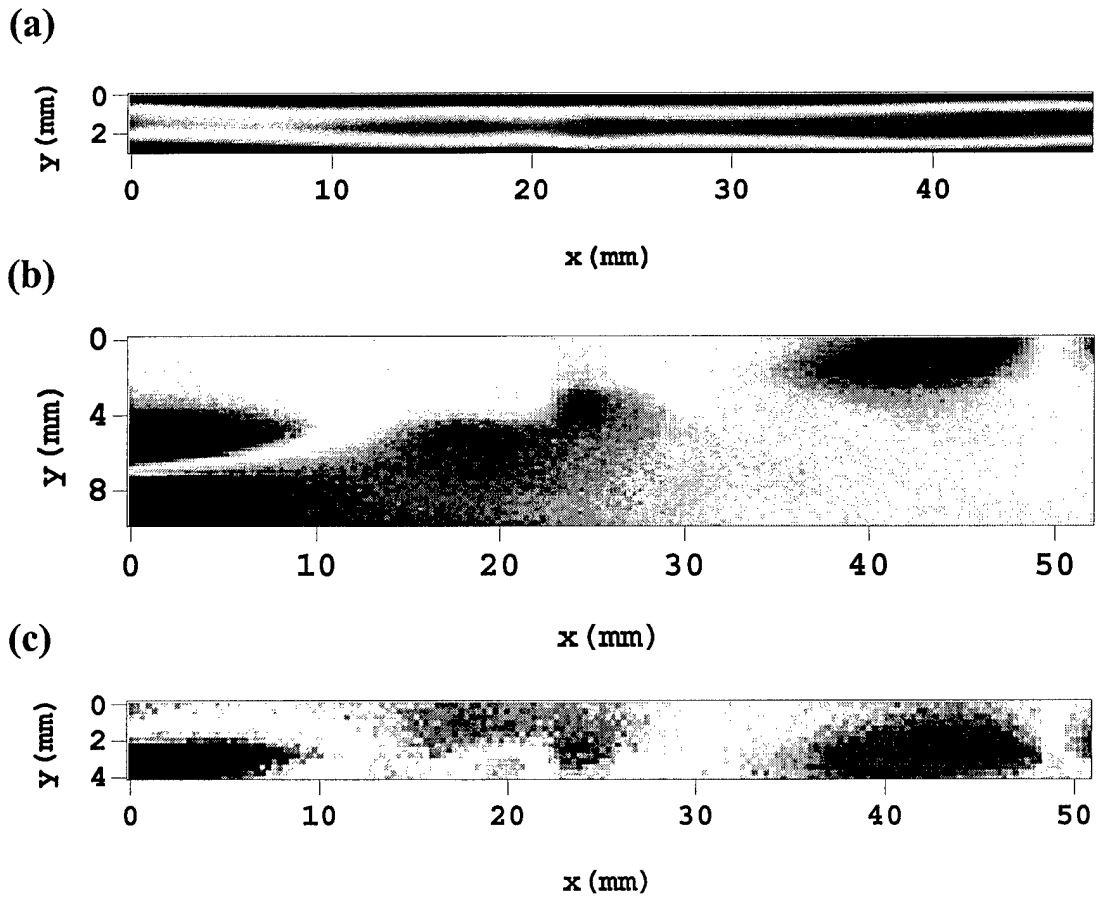

Figure 9.4 Raw magnetic field (B_x) image using the current injected method with (a) normal scanning method and wire aligned along x-scan direction, (b) normal scanning method and wire aligned along the direction of SQUID loop (7.5° tiled), and (c) scanning along the direction of SQUID loop and wire aligned along the direction of SQUID loop.

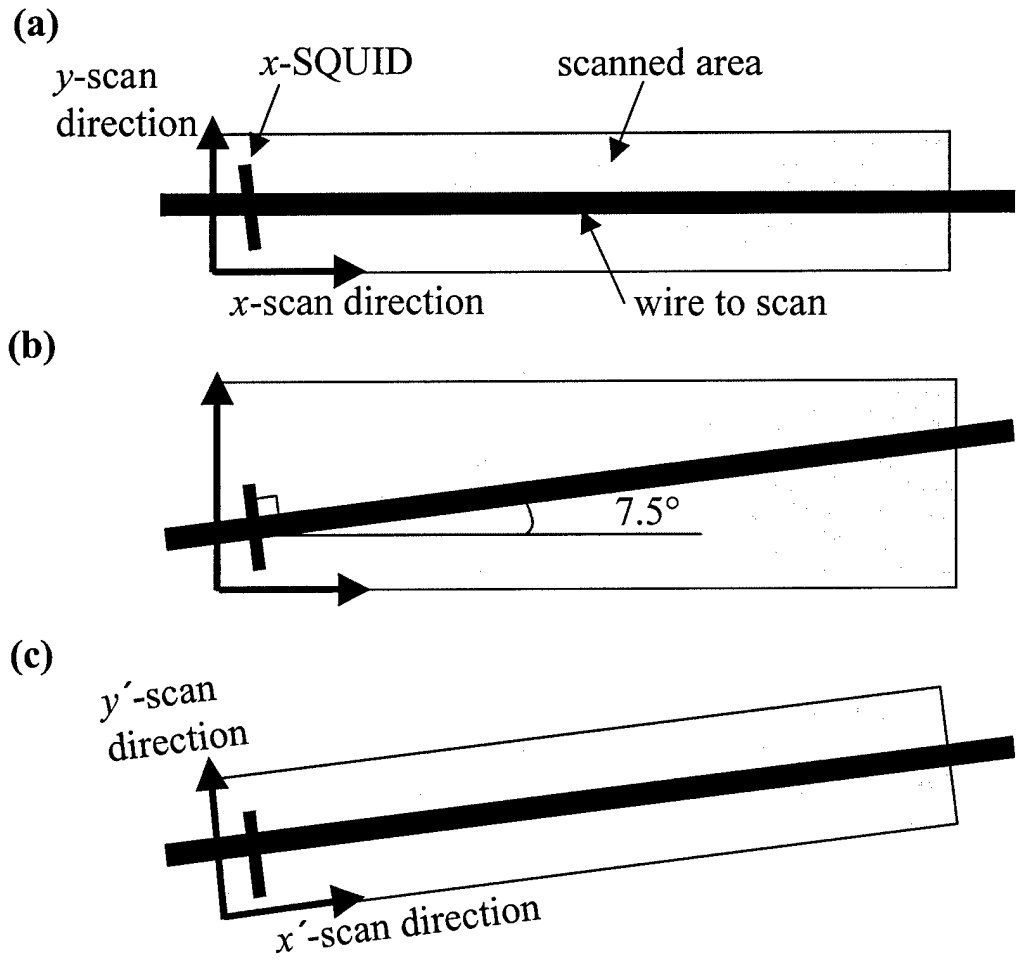

Figure 9.5 Sketch of different set-up of scanning. (a) set-up with normal scanning direction and with wire aligned along x scan direction, (b) set-up with normal scanning direction and with tilted wire, and (c) set-up with tilted scanning direction and tilted wire..

For the experiment, the cylindrical Nb-Ti superconducting wire sample A with the "yield" defect from IGC is used [2]. The injected current in the wire is 20 kHz. Figures 9.4(a)-(c) show the raw magnetic field image from the *x*-SQUID. Actual *x*-SQUID loop is not perfectly

aligned to x-scan direction. Since the tilt angle of the SQUID loop from x-scan direction (see Fig 6.15 and Ch 6.5.2) is about 7.5 degree, the magnetic field image of aligned wire along x-scan direction shows strong signal from wire itself as shown Fig. 9.4(a). Reds/blues indicate 0.6/0.240 μT field gradient respectively. To avoid the signal from the wire itself (not defect), aligning along to the direction of the SQUID loop is required. Figure 9.5 show the sketch of the scanning direction and wire direction corresponding of images in Figs. 9.4. Figure 9.4(b) shows the magnetic field image after the aligning. Reds/blues in Fig. 9.4(b) indicate +0.4/-0.3 μT/mm field gradient respectively. The defect appeared as a red spot in the center in Fig. 9.4(b). Since the wire is tilted compared with scanning direction, the scanning area become larger to cover the wire. To reduce consuming scanning time, I modified the scanning program to move the stage along the tilted wire direction as shown in Fig. 9.5(c). I kept the scanning direction and wire direction in Fig. 9.5(c) for all experiment after this, which is setting the wire tilt as 7.5 degree from x-scan direction and scanning same direction as the tilted wire by moving x and y stage at the same time. Figure 9.4(c) show the result after modifying the scanning program. Reds/blues indicate +80.3/-160.6 nT field gradient respectively. This procedure helps to reduce not only scanning time but also analyzing for the current injection using dB_x/dx (see section 9.5 for detail).

As shown in Fig 9.4(b)-(c), there is strong signal in left and right part of the images. It is same problem as the current injected method with the z-SQUID (I mentioned in previous section Ch 9.2.2). The bending of wire caused the strong signal in the x-SQUID also. To separate the signal from the bending and the defect of the superconducting wire, I use the current injection method using the high-low frequency image subtraction in next section.

9.4 current injection using high-low frequency image subtraction

Depending on the frequency of the current, the penetration depth in the metal is different as shown in Eq. (9.1). Using the property, I can pull out the defect of the wire. Applying high frequency current gives the information of the surface of the metal, while low frequency current give the information of the deep inside of the metal because of long penetration depth. Table 9.1 shows the list of penetration depth varying frequencies for copper and brass. The signal from bending of the wire will be same with high-frequency and low-frequency because the bending occurs in not only the surface but also deep inside of the wire. By subtracting the magnetic field image with high frequency from that with low frequency, the signal from the bending is canceled out but the signal from the defect of the deep inside of the wire is not.

Table 9.1 Penetration depth of copper and brass varying different frequencies.

Freqeuncy (Hz)	ρ_Cu(mm)	ρ_Brass(mm)
500	2.91736	4.21084
1000	2.06288	2.97752
2000	1.45868	2.10542
5000	0.92255	1.33159
10000	0.65234	0.94157
20000	0.46127	0.66579
50000	0.29174	0.42108

9.4.1 Sample B ("seam" defect)

First sample is Nb-Ti superconducting wire with the rectangular cross section with "seam" defect (sample B). Figure 9.6(a) is the raw magnetic field image at 50kHz (Reds/blues indicate +91.5/-53 nT field gradient respectively). It shows large dipole structure. It is known

that the defect is in the center of the dipole structure. However, the signal is very broad, so it is hard to localize. Figure 9.6(b) is the difference field between at 50 kHz and at 1 kHz (Reds/blues indicate +120.5/-120.5 nT/mm field gradient respectively). As shown in Table 9.1, the penetration depth at 50 kHz and 1 kHz are 0.29 mm and 2.062 mm, respectively. It means that the current with 1 kHz can

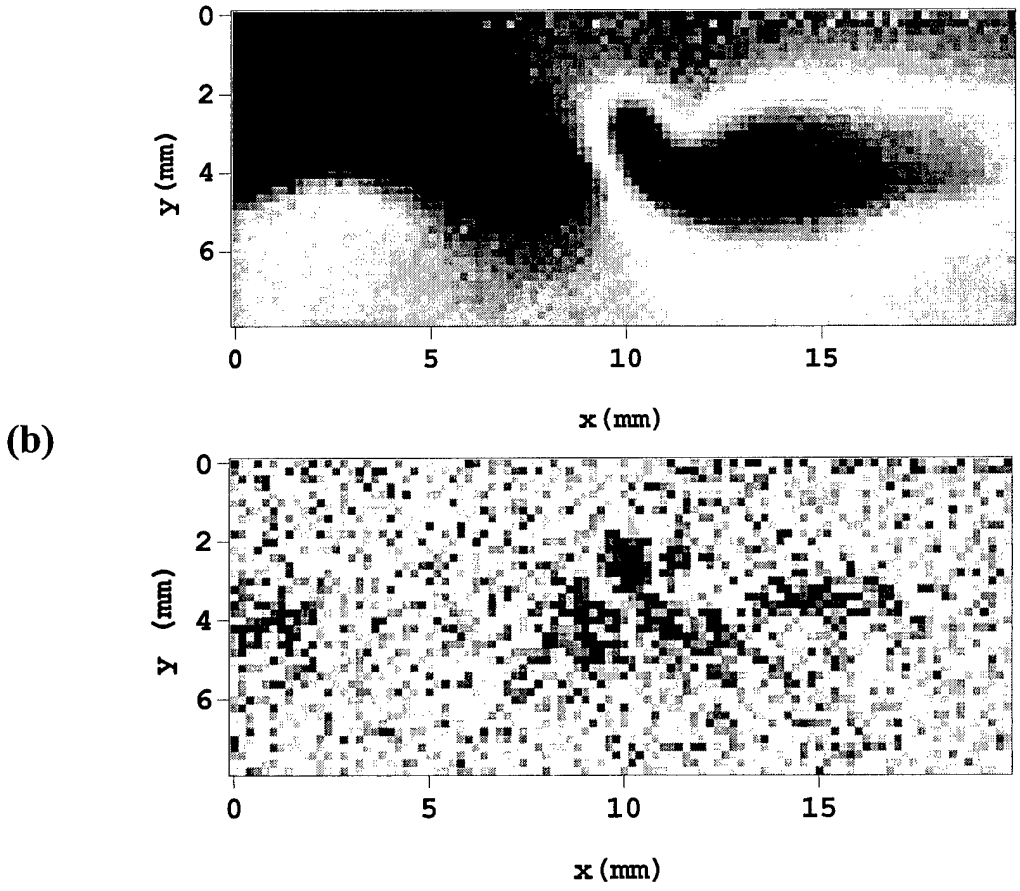

Figure 9.6 (a) magnetic field image B_x and (b) the difference between B_x with 50kHz current and B_x with 10kHz of current injected superconducting wire sample B with the "seam" defect.

penetrate to the deep inside of the wire, but the 50 kHz current cover only surface of the wire. By subtracting these data, I could localize the defect as shown Fig. 9.6(b).

To confirm whether the defect signal of sample B comes from the deep inside or from the surface of the sample, I subtracted images of various frequencies. Figures 9.7(a)-(c) are the differences between 50kHz and 1kHz, 50kHz and 10kHz, and 10kHz and 1kHz, respectively. Figures 9.7(a)-(b) looks very similar showing the defect in the center of wire. However, in Figure 9.7(c) the defect did not appear. It is because the both 10 kHz current (d = 0.653mm) and 1 kHz (d = 2mm) current penetrate into the deep inside of the wire. Therefore, the defect signal is canceled out. It confirm the defect signal is from the deep inside of the wire.

9.4.2 Sample C ("yield" defect)

Figures 9.8 show the magnetic field images of the superconducting wire sample C with the "yield" defect. The raw magnetic field (B_x) appears the defect in the center as shown in the Fig. 9.8(a). By applying same analysis as sample B, I found that the defect signal in the center came from the deep inside of the wire as shown in Figs. 9.8(b)-(c).

By the current injection method using high-low frequency image subtraction, I could distinguish whether it is from bending or from defect. I scanned few more "yield" defects and one "seam" defect, but I could not classify what kind of defect is inside using these method.

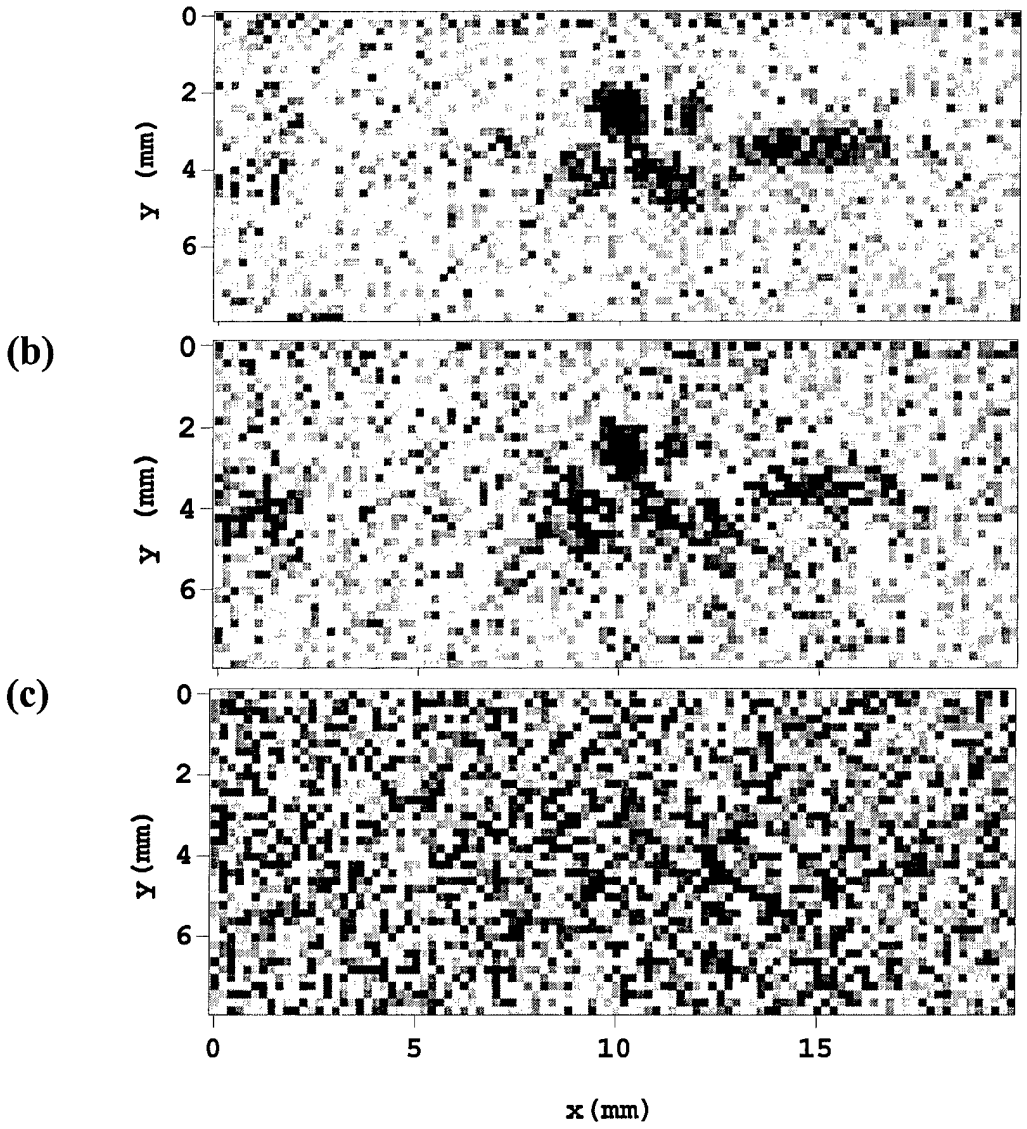

Figure 9.7 (a)-(c) The magnetic field differences between 50kHz and 1kHz, 50kHz and 10kHz, and 10kHz and 1kHz, respectively, of the current injected superconducting wire sample B with the "seam" defect. Reds/blues indicate +120.5/-120.5 nT/mm(a), 84.3/-105.2 nT/mm(b), and 184.7/-168.6 nT/mm(c) field gradient respectively.

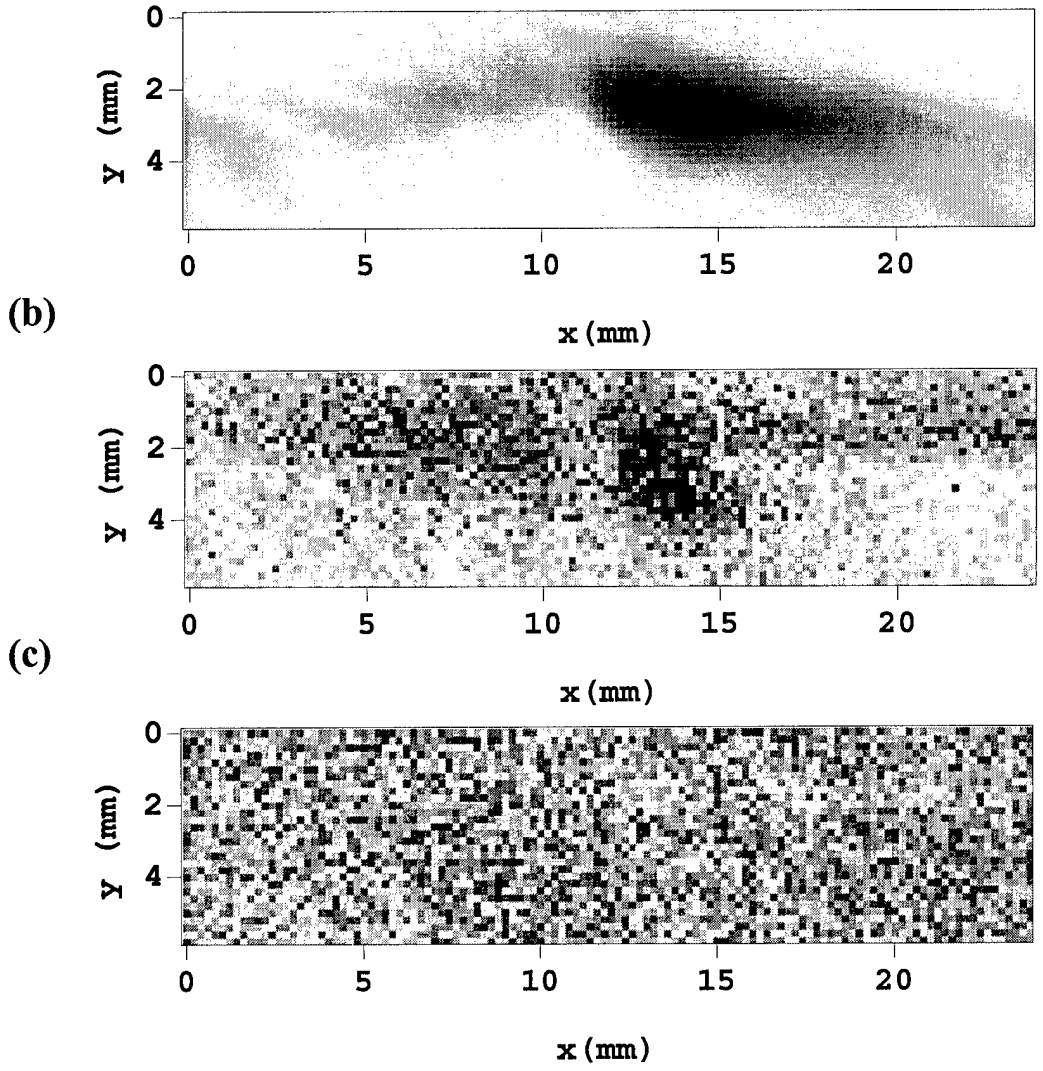

Figure 9.8 (a) magnetic field image B_x, (b) the difference between B_x with 50kHz and 10kHz, and (c) the difference between B_x with 10kHz and 1kHz of current injected superconducting wire sample C with the "yield" defect. Blacks/whites indicate (a) +91.5/-16.1 nT, (b) 321.2/-56.2 nT/mm, and (c) 80.3/-112.4 nT/mm field gradient respectively.

9.5 current injection using dB_x/dx

Taking derivative of B_z with respect to x, E. Fleet could find the defect of the supercoducting wire, but the method could not distinguish signal from the bending or from the defect because the signal from the wire itself (not defect) is very strong in the z-SQUID. In case of the x-SQUID, the signal from the wire itself along the direction of the x-SQUID is negligible. In this configuration, the detected signal is only from the bending or the defect. Since the bending occurs in the wide range compared with the defect size, I can get rid of the signal from the bending by taking the derivative of B_x with respect to x.

9.5.1 Sample A ("yield" defect)

Figure 9.9(a)-(b) is the raw magnetic field image of sample A with 20kHz current. The difference between Fig 9.9 (a) and Fig 9.9 (b) is just flatness. After I scan Fig. 9.9(a), I flattened the wire and scanned Fig. 9.10(b) with same condition. They look different, and it is hard to say where is the defect. However, when I took the derivative with respect of x, I could pull out the defect from both images as shown in Figs. 9.9(c) and (d). The position of the defect in Figs. 9.9(c) and (d) is same.

9.5.2 Sample C ("yield" defect)

Figure 9.10 show comparison of the images of sample C ("yield" defect) with different methods. Figure 9.10(a) is a raw magnetic field B_x using the current injected method, Figure 9.10(b) is dB_x/dx of the image in Fig. 9.10(a), and Figure 9.10(c) is current injected method using 50kHz-10Hz frequency subtraction. The defect appears in

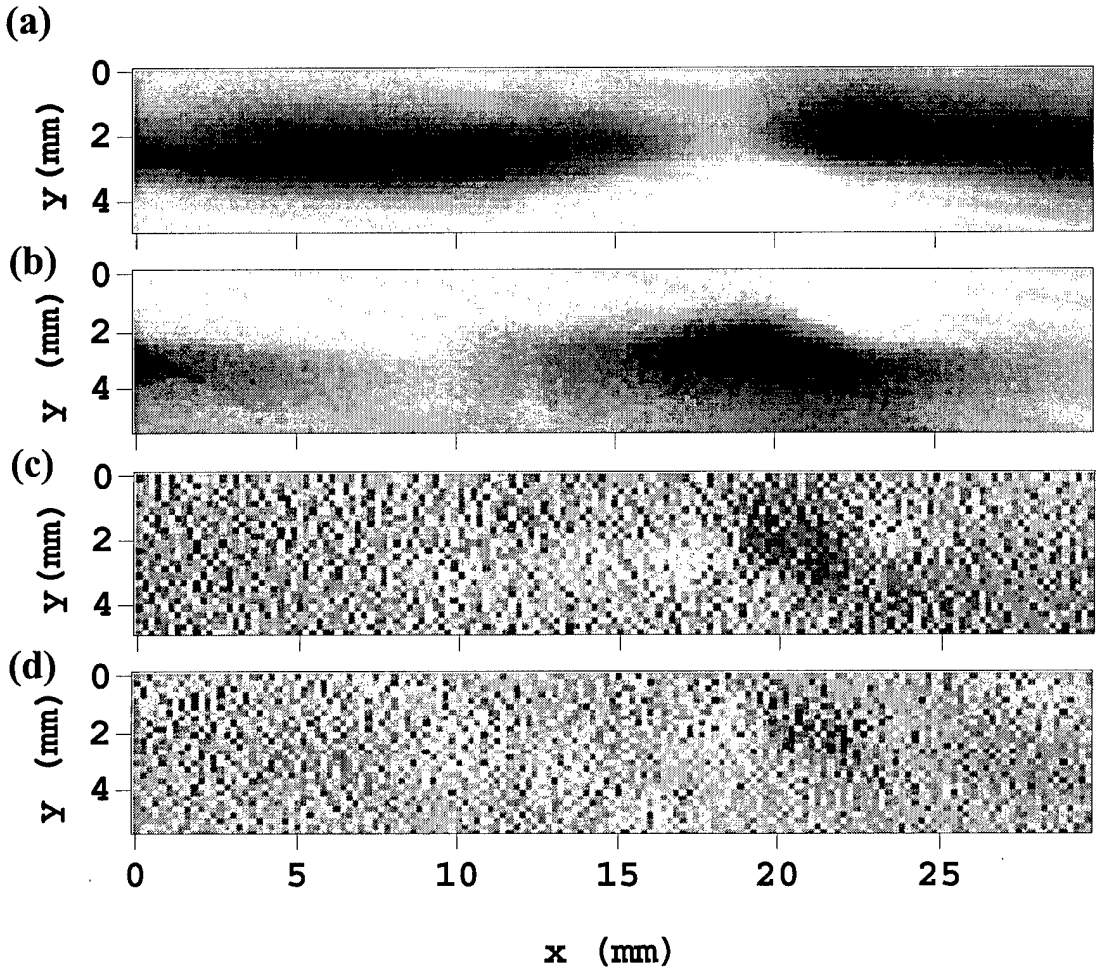

Figure 9.9 (a)-(b) are a raw magnetic field B_x of the current injected sample A with "yield" defect with different flatness. (c)-(d) are the gradient of (a) and (b), dB_x/dx .

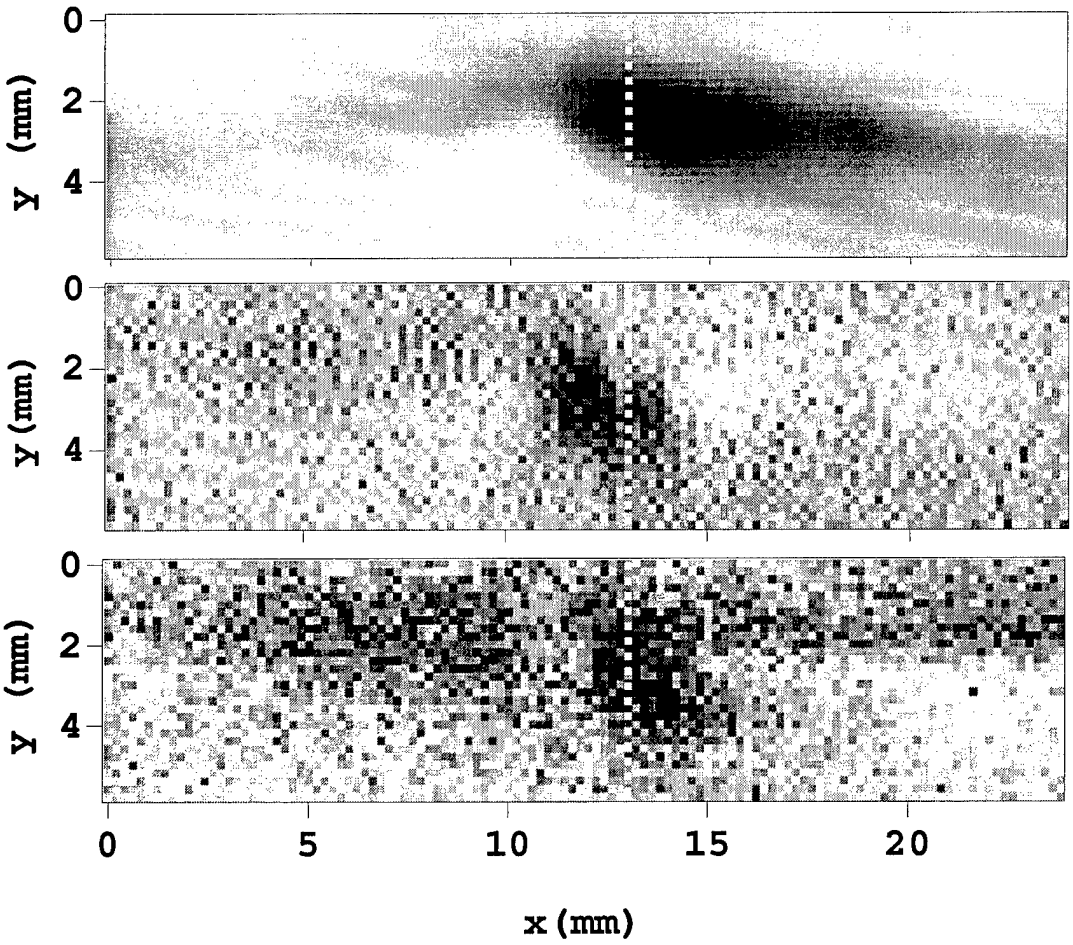

Figure 9.10 (a) is a raw magnetic field B_x of the 50kHz current injected sample C with "yield" defect, (b) is gradient of (a), which is dB_x/dx , and (c) is the magnetic field difference between with 50kHz and with10Hz frequency current injected.

the raw magnetic field image in the Fig. 9.10(a), but the area of the defect is very wide (about 9 mm), so it is hard to localize. The defect in Figs. 9.10(b) and (c) is more localized within 3 mm.

The position of the defect in Fig. 9.10(b) and (c) is at x =11~14 mm and x = 12~15 mm, respectively. The position of the signal from defect in Fig 9.10(b) is about 1 mm off from that in Fig 9.10(c), but it is negligible compared with the wide range of the signal from the defect by other methods.

9.5.3 Sample B ("seam" defect)

Similarly, I took the derivative of the existing magnetic field data with "seam" defect in Fig. 9.6(a). Figure 9.11(a) is a raw magnetic field B_x using the current injected method, Figure 9.11(b) is dB_x/dx of the image in Fig. 9.11(a), and Figure 9.11(c) is current injected method using 50kHz-10Hz frequency subtraction. Similarly with sample C, the signal from the defect in Fig. 9.11(a) is spread widely while the defect signal in Fig 9.11(b) and (c) is more localized. In the sample B, both position of the defect in Fig. 9.11(b) and (c) are placed at 9~11 mm. There is no offset. I note that the signal of the defect using dB_x/dx method in Fig. 9.11(b) is less noisy than that using the high-low frequency subtraction method in Fig 9.11(c).

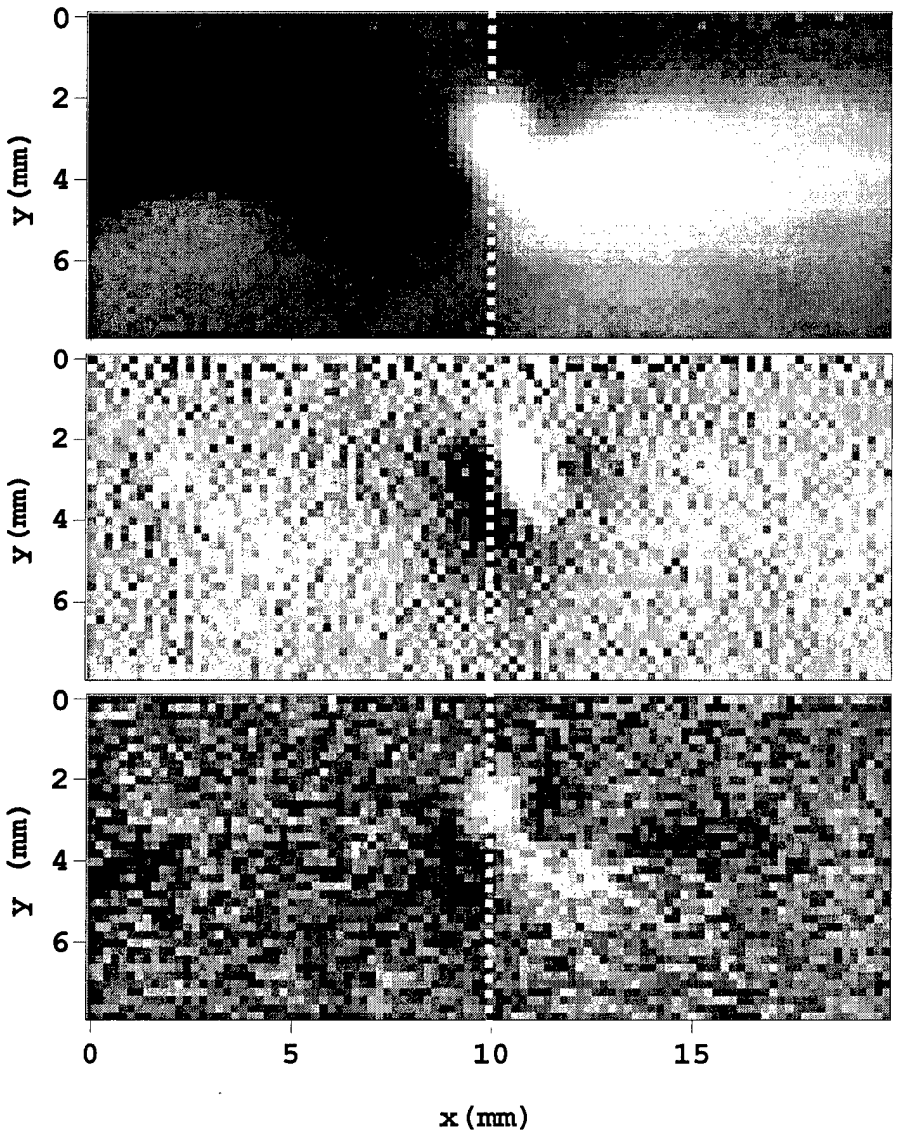

Figure 9.11 (a) is a raw magnetic field B_x of the 50kHz current injected sample B with "seam" defect, (b) is gradient of (a), which is dB_x/dx , and (c) is the magnetic field difference between with 50kHz and with10Hz frequency current injected.

9.6 Fault detection with multi-channel SQUID microscope

Usually the superconducting wire is km-long, therefore it takes too long to check where the defect by area scan. The elapsed time is very important to commercialize the SQUID system for the fault detection of superconducting wire. As shown in Fig. 9.12, if there is a set-up to make the wire in the center of SQUID and move the current injected wire with motor, it is possible to detect the fault by line scan not area scan. However, the thickness of the wire is more than 2mm D. One can increase the SQUID size in order to cover the large area for the thick wire. Then one will lose the spatial resolution. Therefore, the multi-channel SQUID is useful to cover the area of wire and keep good spatial resolution for future fault detecting SQUID system.

Even though I do not have set up for the sample with the step motor as shown in Fig.9.12, I can demonstrate the merit of multi-channel SQUID system by detecting the fault. For the experiment, I use the 4-channel x-SQUID system described in Ch 3-6 to detect the defect of the superconducting wire. First I set up the sample B with the "seam" defect along x' direction (7.5° tilted from x-scan direction) on the scanning stage and made a line scan along x' as shown in Fig. 9.5(c). Since I have 4 channels and the distance between channels is 200 μm, the line scan become area scan, which is 20 mm (length of line scan) × 0.6 mm as shown in Fig. 9.13 (a). The signal from the defect in the raw magnetic field B_x (see Fig. 9.13(a)) has dipole structure and is spread to wide area. Taking derivative of B_x with respect of x, the defect was localized as shown in Fig. 9.13 (b). The range of y is only 0.6 mm in this result, so I couldn't localize the defect in

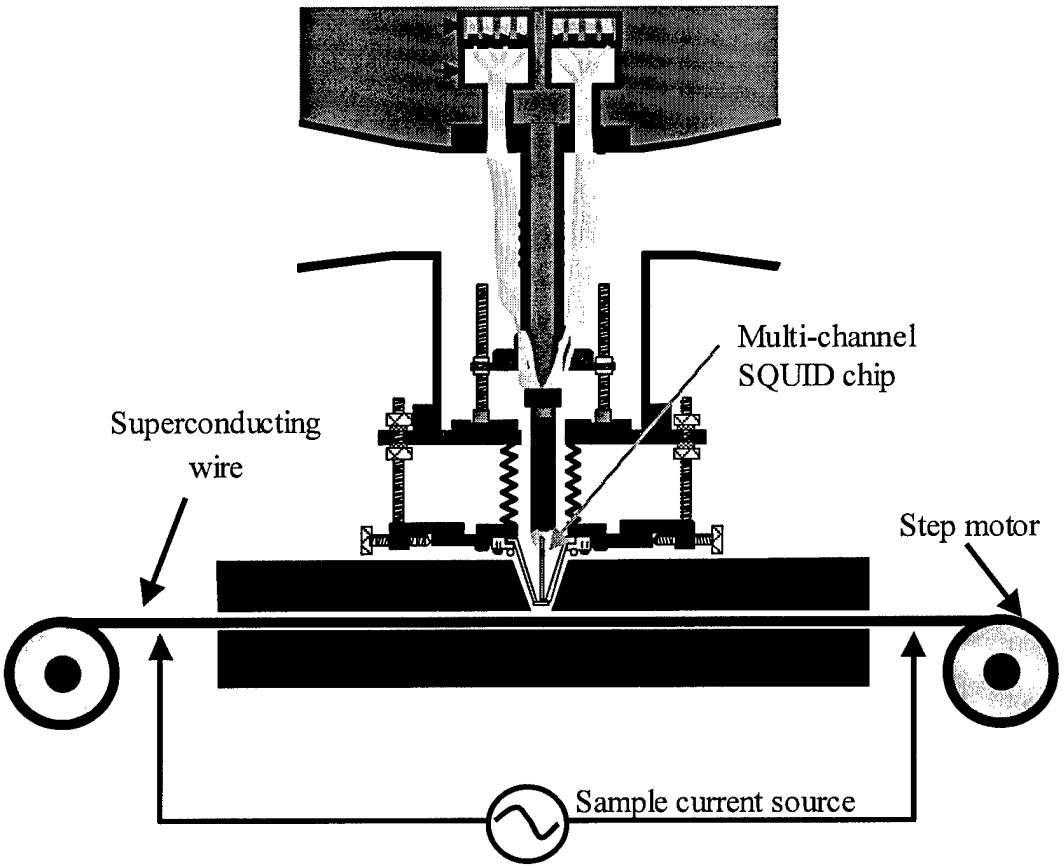

Figure 9.12 Schematic design of fault detector multi-channel SQUID microscope for superconducing wire. (modified from ref [7])

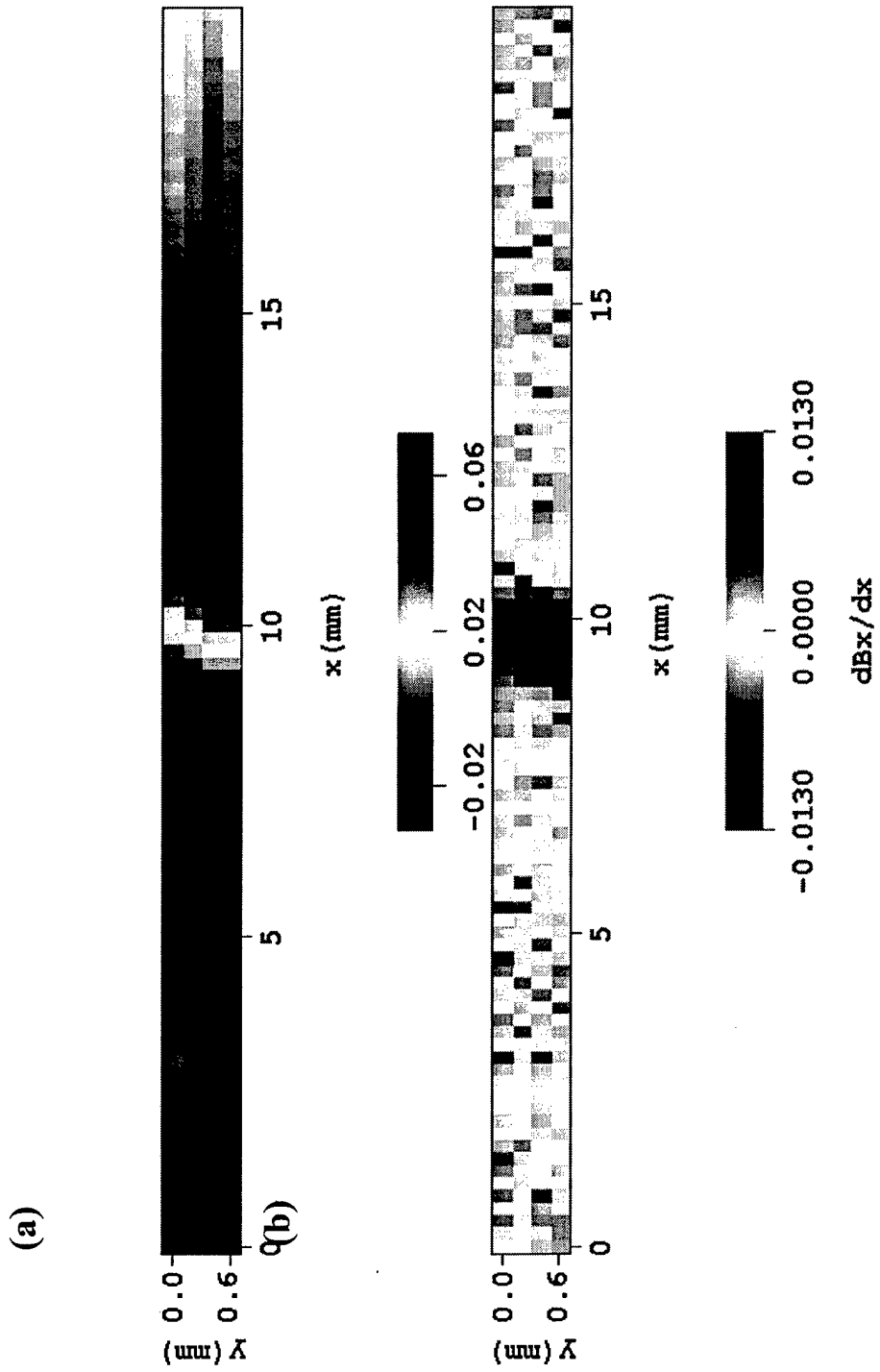

Figure 9.13 (a) line scan of current injected sample B ("seam" defect) by using 4-channel SQUIDs system. (b) gradient of (a).

y- direction. However by using more than 4 channels of SQUIDs with larger distance between channels, I can localize the defect in y-direction.

9.7 Brass test sample with different size holes

Using several methods in previous sections, I can find where the defect is. Now I want to estimate the size of the defect from the magnetic field using x-SQUID. For the experiment, I made Brass test sample with known artificial defect, which are 4 through holes and 4 half-through holes with different diameter (see Fig. 9.14(a)). Since the Brass test sample is very flat, the current injection method appear the defect very clearly. With known defect size, I can find the relation between the measured size from the magnetic field image and the actual defect size at fixed z. As I introduced in section 9.6, if the sample stage for the superconducting wire is built (see Fig. 9.12), then the sensor-to sample distance z will be fixed.

Figure 9.14(b) is the raw magnetic field image using the current injected method. The current flows around the hole and causes x-component of the magnetic field around the holes. That is why there are cloverleaf shapes in the hole. By taking the line section of the strongest magnetic field part of each hole (see Figure 9.14(b)), I can obtain the peak-to-peak distance w as shown is Fig. 9.15. Figures 9.16 (a) and (b) show the actual size of hole vs. responding w of half-through hole and through hole. The diamond shaped dot in Fig. 9.16(a) and the square shaped dot in Fig. 9.16(b) are the averaged experimental results and the dotted lines indicate the fitted result with function,

$$w = a \cdot (\text{actual hole size})^n + b. \qquad (9.2)$$

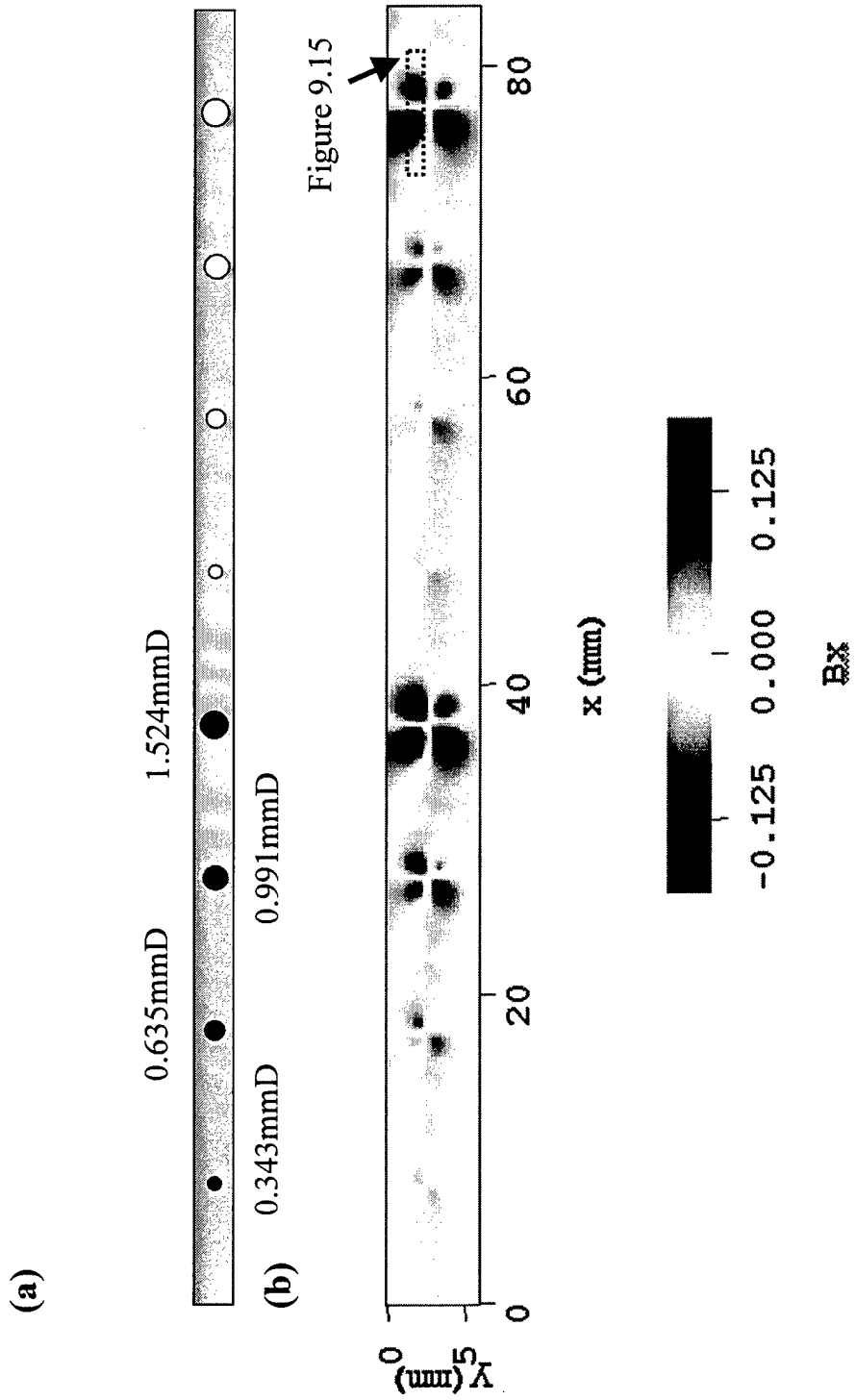

Figure 9.14 (a) Sketch of brass test sample D with 4 half-through holes and 4 through hole having various hole sizes. (b) Raw magnetic field image of current injected sample D.

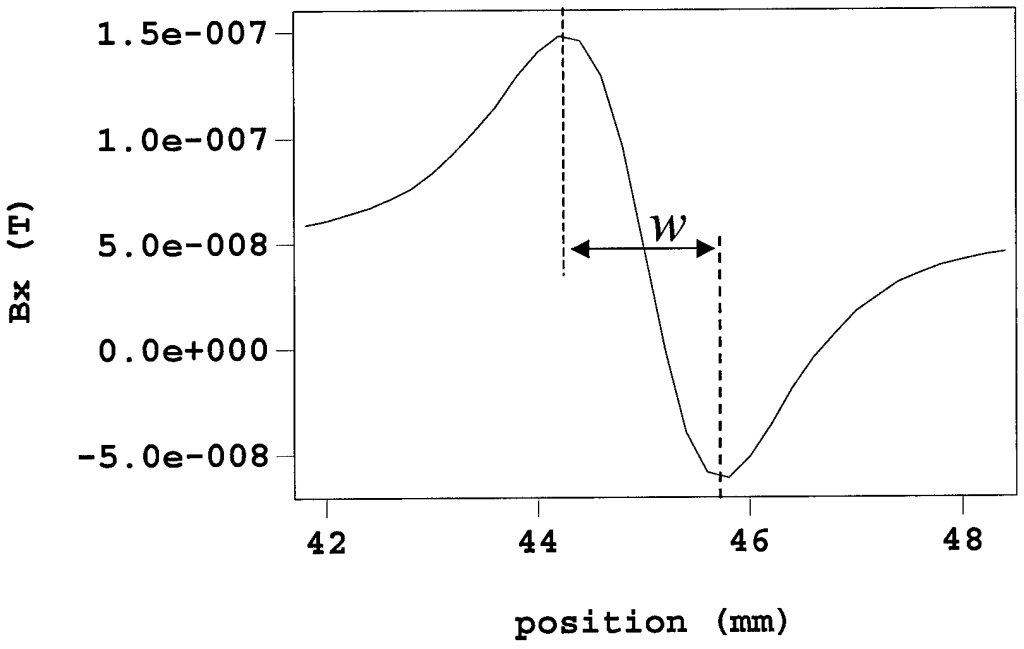

Figure 9.15 line section of dashed marked part in Fig. 9.14, showing how I define "*w*", which is the peak-to-peak distance.

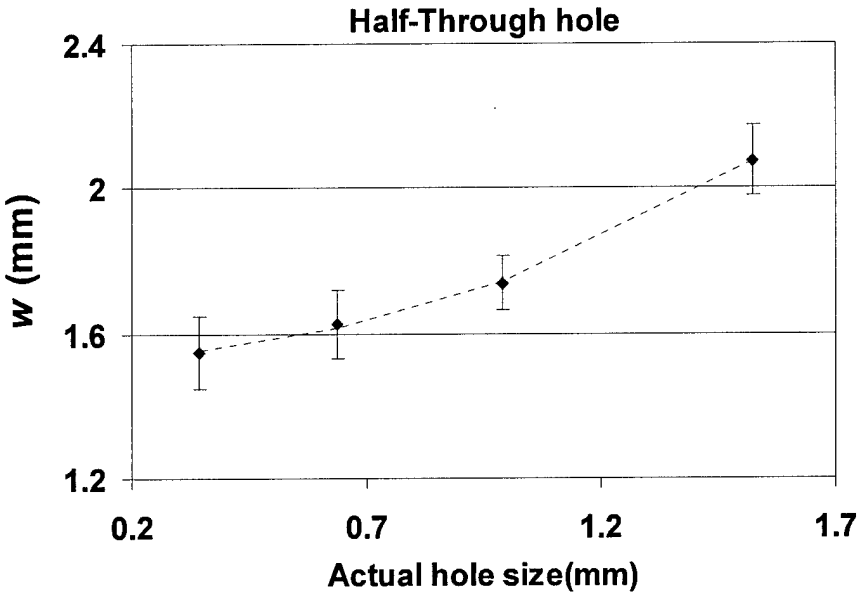

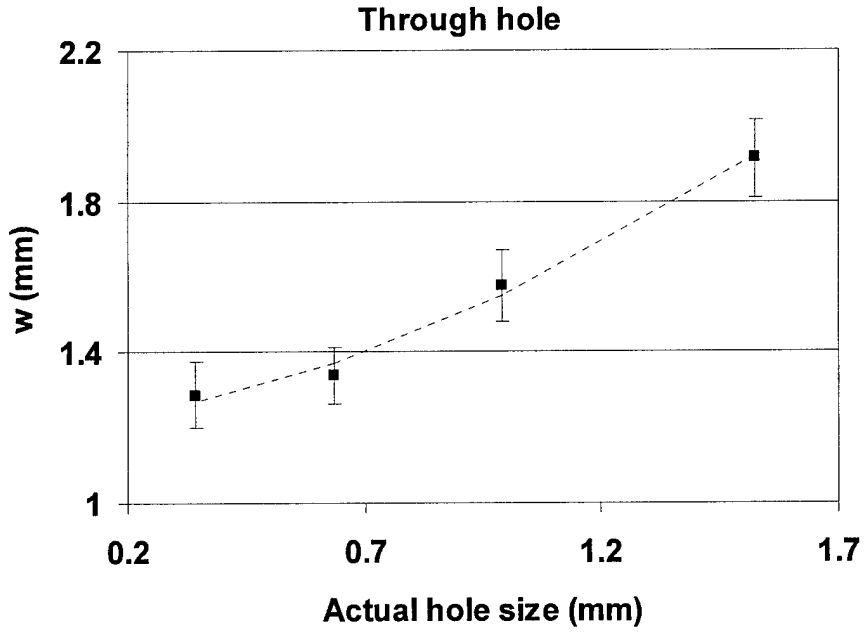

Figure 9.16 Actual hole size vs. measured size w from magnetic field image with (a) half-through hole and (b) through hole.

Table 9.2 is the result of the fitted parameters. The relation between actual hole size and w is not linear but power of n. The n was 2.2 for the half-through hole, while the n for through hole is 1.73. It seams the effect of the half-through hole is larger than the though hole as the size of defect becomes large. The half-through hole is more asymmetric than the through hole. It may cause strong signal as the defect is large. Large error bars in Fig 9.16 (a) and (b) cause large uncertainty of the n. Therefore I can not assure that the fitted n of half-through hole and through hole is right, but I can assure that the n in both case is more than 1 and n for the half-through hole is larger than n for the through hole.

Table 9.2 Fitted result of the half-through holes and through holes using Eq.(9.2).

	half-through hole	through hole
a	0.21	0.34
b	1.54	1.22
n	2.20	1.73

9.8 Conclusion

Using the current injected method with x-SQUID, I could find the defect of superconducting wire. However the signal from the defect is spread to wide area. In addition, the B_x signal was also sensitive to signal from the bending of wire. To solve these problems, I use the current injection method using high-low frequency subtraction and the current injection method taking the derivative of magnetic field B_x with respect to x. Both methods agreed the position of defect and localize the defect within 2-3 mm. By adding more channels of SQUID, I can achieve fast scan of the fault detection without losing the spatial resolution. Finally I found

the measured defect size in the magnetic field image is proportional to (actual size)^n, where n of half-through and through holes are 2.2 and 1.83, respectively.

References

1. E. Fleet, A. Gilbertson, S. Chatraphorn, N. Tralshawala, H. Weinstock, and F. C. Wellstood, "Imaging Defects in Cu-clad NbTi Wire Using a High-Tc Scanning SQUID Microsocpe." *IEEE. Trans. Appl. Supercon.* **11**, 215, 2001.

2. Wire samples were provided by IGC Advanced Superconductors, 1875 Thomaston Ave., Waterbury, CT 06704.

3.E. F. Fleet, "Design and Applications of a cryo-cooled scanning SQUID microscope." *Ph. D. Thesis of University of Maryland*, college park (2000).

4. David J. Griffiths, "Introduction to electrodynamics. 3rd edition", Prentice Hall, 394.

5.E. F. Fleet, "Design and Applications of a cryo-cooled scanning SQUID microscope." *Ph. D. Thesis of University of Maryland*, college park (2000).

6. H. Weinstock, N. Tralshwala, and J.R. Claycomb, *IEEE Trans. Appl. Supercond.* 9, 3797 (1999).

7. H. Weinstock, N. Tralshwala, and J.R. Claycomb, *IEEE Trans. Appl. Supercond.* 9, 3797 (1999).